Microplastics and Nanoplastics

RESEARCH

Open Access

Beyond microplastics - investigation on health impacts of submicron and nanoplastic particles after oral uptake *in vitro*

Maxi B. Paul[1], Christoph Fahrenson[2], Lucas Givelet[3], Tim Herrmann[1], Katrin Loeschner[3], Linda Böhmert[1], Andreas F. Thünemann[4], Albert Braeuning[1] and Holger Sieg[1*]

Abstract

The continuously increasing use of plastics is supposed to result in a rising exposure of MNPs to humans. Available data on human health risks of microplastics after oral uptake increased immensely in the past years and indicates very likely only low risks after oral consumption. Concerning nanoplastics, uptake, transport and potential adverse effects after oral uptake are less well understood. This study aims to investigate differences between microplastic particles and particles in the submicron- and nanoscaled size derived from food-relevant polymers with a particle size range consistent with higher potential for cellular uptake, fate, and effects when applied to human intestinal and liver cells. This work includes the development of cellular and subcellular detection methods for synthetic polymeric particles in the micro- and nanometer-range, using Scanning Electron Microscopy, Small-Angle X-ray and Dynamic Light Scattering methods, Asymmetric Flow Field Flow Fractionation, octanol-water fractionation, fluorescence microscopy and flow cytometry. Polylactic acid (250 nm and 2 µm (polydisperse)), melamine formaldehyde (366 nm) and polymethylmethacrylate (25 nm) were thoroughly characterized. The submicro- and nanoplastic test particles showed an increased uptake and transport quantity through intestinal cells. Both types of particles resulted in observed differences of uptake behavior, most likely influenced by different lipophilicity, which varied between the polymeric test materials. Toxic effects were detected after 24 h only in overload situations for the particles in the submicrometer range. This study provides further evidence for gastrointestinal uptake of submicro- and nanoplastics and points towards differences regarding bioavailability between microplastics and smaller plastic particles that may result following the ingestion of contaminated food and beverages. Furthermore, the results reinforce the importance for studying nanoplastics of different materials of varying size, surface properties, polymer composition and hydrophobicity.

Keywords: Microplastic, Nanoplastic, Oral uptake, Toxicity, Gastrointestinal barrier

Introduction

The potential human health risks associated with exposure to microplastics has become one of the most intensively discussed topics in human consumer protection research, due to constantly rising production, usage and the emissions of plastic to the environment [1]. Plastic in the environment is subject to degradation and fragmentation, which can result in the formation of micron- and nano-sized plastic particles, commonly referred to as micro- and nanoplastic particles (MNPs). Furthermore, the use of intentionally added MNPs in consumer products, commonly referred to as primary microplastics, can result in the direct environmental release of micron-sized plastic particles [2–4]. As an environmental contaminant in air and water, exposure for humans to MNPs can occur either via inhalation and/or dietary uptake [5], through e.g. drinking water, beer, salt, seafood, honey

*Correspondence: Holger.Sieg@bfr.bund.de

[1] Department of Food Safety, German Federal Institute for Risk Assessment, Max-Dohrn-Str. 8-10, 10589 Berlin, Germany
Full list of author information is available at the end of the article

and beverages [6]. The use of primary MNPs are not understood to represent a significant mass-based fraction of exposure [7]. They are mainly used for medical and research purposes or can emerge through decomposition of larger particles (i.e. secondary microplastics) as a result of weathering and/or ageing processes [7, 8]. With respect to human exposure to MNPs, recent studies suggests a total weekly exposure of as much as 0.1–5 g of MNPs, with the higher estimates of exposure suggested to be above the 99th percentile of human exposure [9, 10].

While estimates of exposure based on the mass of MNPs potentially vary several orders of magnitude, less is understood regarding the number of MNPs that such an exposure represents. The number of particles at lower particle sizes, for instance, may potentially be several orders of magnitude [11–13], although the mass of nanoplastic particles may be relatively small. On the other hand, exposure to larger numbers of microplastics >150 µm, for instance, may be relatively low [3], but the mass for these particles will be larger and potentially dominate the total mass-based estimates of exposure. For nanoplastics, there are no data reporting environmental exposure, largely because there are no validated detection methods and no reference materials available. Since the physiological toxicity of MNPs will likely differ depending on particle size, shape, surface area and polymer composition, there is a need to better understand both exposure to MNPs and the associated toxicities, particularly for MNPs <10 µm [14–16].

Knowledge of cellular uptake and toxicity of MNPs of varying size, shape and polymer composition represents a current research need [17]. It is still unclear, whether these particles behave differently with regard to their cellular uptake and possible toxicological impact. Previous research has mainly focused on Polystyrene (PS) microplastic spheres [6, 8, 18], even though it is understood that PS does not represent the most abundant types of MNPs observed in the environment, which is better characterized as representing a heterogeneous mixture of particle sizes, shapes and densities [19]. The intestinal cellular and systemic uptake of MNPs >10 µm are reported to have a lower probability than MNPs <1.5 µm [7]. In some cases, however, particles up to 150 µm, have been observed in organs, such as the liver, possibly via a paracellular transport mechanism, referred to as persorption [20]. Particles >150 µm, however, are not considered to have biological impact on human health, due to their low reactivity. Toxic effects arised from *in vitro* experiments are often only documented in so-called overload situations, which are distinguished by the use of a high excess of particles [8]. To date, the potential effects associated with exposure to MNPs are inflammation, oxidative stress, apoptosis and effects concerning metabolic homeostasis, which can be caused by unspecific cellular stress reactions [6].

Recognizing there exists a need to expand our understanding of the uptake and toxicity of MNPs of environmentally relevant polymers, in this we used fluorescently labeled particles of the food-relevant materials melamine formaldehyde (MF), polylactic acid (PLA) and polymethylmethacrylate (PMMA). MF is used for the production of baking- and kitchenware, as well as for bambooware and as coating material. PLA is used for multiple applications, such as in beakers, bottles or foils. PMMA occurs, for example, in transparent kitchenware, such as bowls, salad spoons and pepper grinders. As a consequence of mechanical use, ageing or damage, particles of varying size have the potential to be released into food and beverages and can subsequently be ingested [5]. In this study, all applied particle species are expected to contain particles <1 µm, and which enables a comparison of effects for particles of different sizes and materials, aimed at providing better mechanistic understanding of the behavior of MNPs. The definition and categorization framework of MNPs is still an unresolved debate that can lead to misunderstandings when interpreting results arising from MNP research studies. While Hartmann et al. have suggested nanoplastic particles refer to dimensions <1 µm [21], we have decided to use the term "nano" as commonly used in the nanotoxicology field [22], whereby nanoplastic refers to particles in the size range 1–100 nm. In literature, there is often a gap in the definition between the lower size limit for microplastics (>1 µm) and the size range for nanoparticles below 100 nm. To emphasize this for the test plastic particles with diameters between 100 and 1000 nm we use the term "submicron".

The particles generated and used in this study are thoroughly characterized and the toxicity assessed using intestinal and liver cells. Supporting the toxicity assessment, cellular interaction of particles with Caco-2 cells (mimicking the intestinal barrier), HepaRG and HepG2 cells (mimicking liver cells) as well as transport through the intestinal barrier are quantified [23, 24]. The overall aim of this study, therefore, is to identify any substantial differences between microplastics and smaller particles with regard to their cellular uptake, fate and effects.

Methods/experimental

Chemicals and plastic particles

All chemicals were purchased from Merck (Darmstadt, Germany), Carl Roth (Karlsruhe, Germany), Sigma-Aldrich (Taufkirchen, Germany) if not stated otherwise. The 366 nm MF particles "MF366" (charge: MF-FluoOrange-S886–1, Ex/Em 560 nm/584 nm) were purchased from Microparticles GmbH (Berlin,

Germany), both PLA particle types (250 nm and 2 µm) "PLA250" and "PLA2000" (PLA-greenF, prod.-no: 51–00-252 and 51–00-203, Ex/Em 502 nm/527 nm) were purchased from Micromod particle technology GmbH (Rostock, Germany) and 25 nm PMMA particles "PMMA25" (DiagPoly™ Plain Fluorescent PMMA nanoparticles, cat.-no.: DNG-P010) were purchased from Creative Diagnostics (New York, USA). The 10 µm PS particles (prod.-no.: PFH-10056, Ex/Em 530 nm/582 nm) were bought from Kisker Biotech GmbH (Steinfurt, Germany), the 4 µm PS particles (prod.no.: 2219, Ex/Em 530 nm/582 nm) from Phosphorex Inc. (United States) and the 1 µm PS particles (prod.no.: F13080, Ex/Em 505 nm/515 nm) were purchased from life technologies (Carlsbad, Germany). When investigating MNPs, it is important to distinguish between effects caused by the material, dispersant, the size and/or the surface. Especially the dispersant can play a role in evoking adverse effects on cells, which underlines the importance of having an adequate set of controls [25]. To ensure any dispersant-related effects were excluded in this study, all particles were delivered as aqueous dispersions. An overview about the purchased plastic particles and the applied methods can be found in the supporting information (Table S1).

Characterization of particles

Plastic particles were characterized using Fluorescence Microscopy, Scanning Electron Microscopy (SEM), Dynamic Light Scattering (DLS), Asymmetric Flow Field Flow Fractionation (AF4), Small-Angle X-ray Scattering (SAXS) and assessing an octanol-water distribution coefficient (hydrophobicity).

Fluorescence microscopy

To check for particle size, shape and fluorescence signal, stock plastic dispersions were analyzed in their stock concentrations using the inverse microscope axio observer d1 (Carl Zeiss, Oberkochen, Germany). Images were recorded using Brightfield, EGFP (Ex/Em 488/509) or Cy5 (Ex/Em 650/673 nm) filter depending on the wavelength of the particles label.

SEM

For precise verification of particle sizes and shape, pristine plastic dispersions were analyzed using a Zeiss DSM 982 Gemini (Carl Zeiss AG, Oberkochen, Germany; updated by point electronic GmbH, Halle (Saale), Germany) conducted with an acceleration voltage between 6 and 9 kV as described in a study using microplastics before [23]. Size distribution was quantified on the basis of the SEM images by using the ImageJ software V.1.53 (Laboratory for Optical and Computational Instrumentation (LOCI) of the University of Wisconsin-Madison, Madison, USA). The Feret diameter was determined by using the function 'Measure' and measuring at least 200 random particles per type. The scale bar of the SEM images was used to define a scale in the program. Results are shown as histograms.

DLS

Hydrodynamic diameter and zeta potential were measured with a Zetasizer Nano ZS (Malvern Panalytical GmbH, Kassel, Germany). Plastic particles were diluted 1:1000 in ultrapure water and subsequently measured. Results for hydrodynamic diameters are given as size distribution curves and polydispersity indices. For zeta potential, the universal 'Dip' Cell Kit (Malvern Panalytical GmbH, Kassel, Germany) was used. Mean values and standard deviations of at least three measurements were calculated. Since experiments were performed in cell culture media, further DLS measurements in medium at 20 °C and 37 °C and for incubation time points of 0 h and 24 h were performed.

AF4

Particle sizes were further determined by AF4 coupled to Multi Angle and Dynamic Light Scattering (MALS/DLS) for all particle types except of PLA2000. The AF4 system consisted of an Agilent 1200 series autosampler (G1329A), a high-performance liquid chromatography pump (G1311A) (Agilent Technologies, Santa Clara, CA, USA), an Eclipse 3 AF4 flow control module, and a short channel-type AF4 separation channel with a 350 µm spacer (Wyatt Technology Europe GmbH, Dernbach, Germany). The carrier liquid was ultrapure water containing the alkaline detergent mix Fisherbrand FL-70 (Fisher Scientific, Pittsburgh, MA, USA) at a concentration of 0.025% (v/v) or ReagentPlus sodium dodecyl sulfate (SDS, Sigma Aldrich, St. Louis, MO, USA) at a concentration of 0.05% (m/v). Following separation by AF4, a DAWN HELEOS TM (Wyatt Technology Europe GmbH, Dernbach, Germany) MALS detector with 17 observation angles operated with a linear polarized laser light at 658 nm was used to record the light scattering signal. The data collection interval was set to 2 s. A DLS detector at angle 99° of the DAWN HELEOS light scattering cell was used for on-line determination of the hydrodynamic diameter d_h of the particles with an interval of 1 s. Data from the light scattering detectors was processed using the ASTRA V software (version 5.3.4.20, Wyatt Technology Corporation, Santa Barbara, CA, USA). The MALS detector at angle 90° was used for light scattering detection of the particles. The root mean square (rms) diameter d_{rms} was determined using a 3rd order Debye model because of its robustness and fitting

capabilities for both spherical and non-spherical particles [26]. Before analysis, the samples were diluted in carrier liquid 1:500 (PLA250, MF366) or 1:50 (PMMA25). The instrumental settings are presented in Table S2.

SAXS

The goal of the SAXS measurements was to determine the size distribution of the particles *in situ.* Measurements were performed in a flow through capillary with the Kratky-type instrument SAXSess (Anton Paar, Graz, Austria) at 21 ± 1 °C. The SAXSess has a low sample-to-detector distance of 0.309 m, which is appropriate for investigation of dispersions with low scattering intensities. The samples were measured as delivered. The scattering vector q depends on the wavelength λ of the radiation ($\lambda = 0.154$ nm): thus $q = 4\pi / \lambda \sin\theta$. Deconvolution (slit length desmearing) of the SAXS curves was performed with the SAXS-Quant software. Curve fitting was conducted with software SASfit as described earlier [27]. The analysis of the SAXS raw data was performed using forms presented in the supporting information.

Hydrophobicity

To elucidate the distribution of plastic particles in hydrophilic or lipophilic phases and exclude experimental leaching effects, an octanol-water-distribution was assessed. Respective plastic particles were diluted 1:10 in ultrapure water, mixed in equal amounts with octanol and vortexed for 10 sec. Phases were separated again by shortly spinning the dispersion in a table centrifuge. The content of particles in the hydrophilic and lipophilic phase was measured using the Tecan plate reader (Plate Reade *Infinite*® M200Pro. Tecan Group Ltd., Männedorf, Switzerland). Another 1:2 dispersion of diluted particles with octanol was mixed for 24 h at room temperature. The fluorescence intensity of the phases was measured again. The two phases were ultracentrifuged at 186000 x g for 40 min and the fluorescence of the supernatant measured, but no significant fluorescence was detected (data not shown).

Cell cultivation

Caco-2 (ECACC: 86010202) and HepG2 (ECACC: 85011430) were purchased from the European Collection of Authenticated Cell Cultures (Salisbury, UK). HepaRG cells were obtained from Biopredic International (Saint Grégoire, France). The cells were cultivated as published before [23, 28]. Cultivation of cells was performed at 37 °C and 5% CO_2. Caco-2 and HepG2 were cultured in Dulbecco's Modified Eagle Medium (DMEM; Pan-Biotech GmbH, Aidenbach, Germany) supplemented with 10% fetal calf serum superior (FCS superior), 10^5 Units/L penicillin and 100 µg/mL streptomycin (P/S; Capricorn Scientific GmbH, Ebsdorfergrund, Germany). HepaRG cells were cultured in Williams E medium (Pan-Biotech GmbH, Aidenbach, Germany) supplemented with 10% FCS (Pan-Biotech GmbH, Aidenbach, Germany, 1% P/S, 0.05% of 100 µg/ml human insulin (PAA Laboratories GmbH, Pasching, Austria), and 50 µM hydrocortisone-hemisuccinate (Sigma-Aldrich, Taufkirchen, Germany). These cells were passaged every 2 weeks. Caco-2 and HepG2 were passaged every 2–3 days at 80–90% confluence. This was conducted by aspirating the cell culture medium, washing the cells with phosphate-buffered saline (PBS) and subsequently incubating them with 0.05% of trypsin-ethylenediaminetetraacetic acid (EDTA) at 37 °C for 5 min (Caco-2) or 7 min (HepG2). Followed by adding 8.5 ml cell culture medium and centrifuging the cell suspension. The cell pellet was resuspended in fresh cell culture medium.

Cell viability testing

Caco-2, HepG2 and HepaRG cells were seeded in 96-well plates with concentrations of 5000 (Caco-2), 20,000 (HepG2) and 9000 (HepaRG) cells per well in their respective cell culture medium. HepG2 cells can be used for experiments 24 h after seeding. Caco-2 and HepaRG cells were differentiated for 3 weeks and 4 weeks, respectively. The HepaRG cells were cultivated in their cell culture medium for 2 weeks and further differentiated for another 2 weeks by adding 1.7% Dimethylsulfoxide (DMSO, v/v) to the proliferation medium. To perform the incubation, cell culture medium was replaced by 100 µL phenol red-free cell culture medium containing different concentrations of plastic particles. The maximum concentration was chosen to exclude effects due to nutrient deficiency of cells, while at the same time ensuring concentrations would result in toxic effects being observed. The unit μm^2 particle surface/mL was used to apply concentrations with comparable particle surface area exposed to the cells and to therefore exclude toxic effects based on the increasing surface-to-volume ratios of the smaller particles. To achieve comparability, the resulting concentrations in particles/mL and the conversion factor are presented in Table S3. After 24 h or 48 h of incubation, the particle dispersions were aspirated and substituted by 100 µl phenol red-free medium and the 3-(4,5-dimethylthioazole-2-zyl)-2,5-diphenyltetrazolium bromide (MTT) assay was performed, as previously described [23], to determine the metabolic activity of cells after incubation with plastic particles. A 5 mg/mL solution of MTT in PBS was thus added at a volume of 10 µL per well and incubated for 1 h. The supernatant was removed afterwards and 130 µL per well of a desorption solution containing 0.7% (w/v) SDS in isopropanol was added. The 96-well plates were shaken for another 30 min

under light exclusion to dissolve the formazan crystals. Absorption was measured at 570 nm and 630 nm background absorption. A concentration 0.01% Triton X-100 was used as positive control. To evaluate the results, raw data were subtracted by background signals (wells that were incubated with corresponding particle concentrations and all assay components, but did not contain cells and the medium control). This value was related to the solvent control (cells incubated with cell culture medium, but no particles), which was set to 100%. Mean values and standard deviations were calculated for at least three independent experiments.

To test the cell viability for longer incubation times, the xCELLigence® Real Time Cell Analysis (Agilent Technologies Germany GmbH & Co. KG, Waldbronn, Germany) was used on the basis of a protocol published earlier [29]. Caco-2, HepG2 or HepaRG cells were seeded as explained above on special 96-well microplates, coated with gold microelectrodes. Cells were differentiated and incubated with 150 µL of particle dispersions in cell culture medium diluted to different concentrations (ranging from 5×10^7–2.5×10^{10} µm^2 particle surface/mL. The cell index was measured every hour for 72 h in total. 50 µg/mL zinc oxide (ZnO) served as positive control.

Particle uptake and transport through the intestinal barrier and uptake in hepatic cells

Intestinal barrier

To verify the particle uptake and transport through the intestinal epithelium, 12-well Transwell® plates consisting of polycarbonate membrane inserts with 1.12 cm^2 growth area and 3 µm pore size (Corning Incorporated, New York, USA) were used, based on a protocol established by Stock et al. [23]. Short, 50,000 Caco-2 cells were seeded on top of the membrane of the Transwell® inserts and differentiated for 3 weeks. The cell culture medium was changed every two or three days. To check for the permeability of the monolayer of Caco-2 cells, transepithelial electrical resistance (TEER) measurements and transport of fluorescein isothiocyanate-dextran (FITC) were applied. Permeability values > 700 Ω*cm^2 (TEER) and < 10^7 cm/s (P_{APP} values calculated from FITC transport) demonstrated the overall integrity of the Caco-2 monolayer. After three weeks of differentiation, cells were incubated with high, but non-toxic concentration (determined beforehand by cell viability tests) of plastic particles for 24 h in the apical compartment or with cell culture medium as a control. This was performed by removing the cell culture medium and replacing by a 500 µl particle dispersion that was diluted to a concentration of 2.5 µm^{2}x10^9 µm^2 particle surface/mL in the apical side and 500 µl cell culture medium without particles in the basolateral side. Afterwards, the apical and basolateral, as well as washing fractions (2 × 250 µL PBS), were collected and fluorescence intensity for each particle type measured at the Tecan plate reader. To be able to quantify the signals, calibration curves of the particles in respective medium (cell culture medium or PBS) were prepared and measured with the Tecan plate reader. The highest selected concentration was the initial particle concentration used for incubation. The Transwell® membranes were fixed with 3.7% formaldehyde solution in PBS for 30 min at 37 °C. In the next step, the fixed membranes were washed three times with PBS and the whole membrane was scanned with the Tecan plate reader to determine the fluorescence signals present in the membranes. By adding known amounts of the particle concentrations used for incubation and measuring the increase of the fluorescence, a standard curve was calculated. Afterwards, membranes were washed again three times with PBS.

To examine the interaction (comprising cellular uptake and adsorption) of the particles with the Caco-2 cells, a confocal microscope (Leica TCS SP5, Leica Microsystems GmbH, Wetzlar, Germany) was used. The fixed and washed Transwell® membranes were further prepared by permeabilization with 0.2% Triton-X 100 in PBS for 20 min. After washing for three times with PBS, the cells were stained with 2 drops/mL ActinGreen 488 ReadyProbes® Reagent (wells incubated with MF particles) or 2 drops/mL ActinRed 555 ReadyProbes® Reagent (wells incubated with PLA or PMMA particles; Life technologies, New York, USA) for 30 min under light exclusion. In the last step, the membranes were washed three times with PBS and the insert was cut off by using a scalpel. The membrane was fixed on a microscope slide by using Kaiser's glycerin gelatin (Carl Roth GmbH + Co. KG, Karlsruhe, Germany) and cover glasses. The samples were dried over night at 4 °C and examined on the next day. For each particle type, five random sections of the membrane from 2 to 3 replicates per particle were investigated. Due to resolution limits of the confocal microscope, sections were not quantified. Images were recorded by using the XYZ acquisition mode and the contrast was adjusted. This shows the membrane from its lateral side starting from the villi of the cells and ending at the membrane.

Hepatic cells

To check for uptake of plastic particles into hepatic cells, fluorescence microscopy was used with HepG2 and HepaRG cells [29]. Since HepG2 are proliferating hepatocyte-like cells without the capability of expressing enzymes of the xenobiotic metabolism and HepaRG are differentiated bilary- and hepatocyte-like cells expression Phase I and Phase II enzymes, a comparison of different uptake

based on the cell models complexity. Therefore, HepG2 or differentiated HepaRG cells were incubated with high, but non-toxic concentrations of respective MNPs for 24 h. Cells were washed twice with PBS to remove particles laying on top of the cells. For microscopic examinations, cells were covered with PBS and the uptake of particles was assessed using an Axio Observer D1 (Carl Zeiss, Oberkochen, Germany). Images were assessed using Bright, EGFP and Cy5 filter dependent on the particles label.

Flow cytometry

To establish a flow cytometry-based method to study uptake of plastic particles in liver cells, only HepG2 cells were used due to their easier handling in comparison to HepaRG cells. The protocol was based on a previously published study [29]. The efficacy of the method was evaluated by characterizing the uptake of previously studied PS particles in the micrometer size range (10 µm, 4 µm, 1 µm) and at concentrations of 2.5×10^8 μm^2 particle surface/mL, and then applied to the other test particles used in this study. Differentiated cells were incubated for 2, 4, 6 and 24 h, respectively to trace the increase of particle uptake with time at concentrations of 5×10^8 μm^2 (PLA2000), 2.5×10^9 (PLA250), 2.5×10^8 μm^2 (MF366) and 2×10^{11} (PMMA25) particle surface/mL, dependent on the particles toxicity on HepG2 cells. After washing the cells twice with PBS, the incubated cells were subsequently harvested using trypsin-EDTA. The cell suspension was centrifuged at 300 x g for 5 min, resuspended in 100 µL PBS and used for measurements. To do so, the flow cytometer BD Accuri C6 (BD, Heidelberg, Germany) was utilized with an excitation laser at 488 nm. The optical filters FL1 (533/30 nm), FL2 (585/40 nm) or FL3 (> 670 nm) were used dependent on the fluorescence of the particles. Signals were detected for 2 min or a maximum of 10,000 cells. For analysis, the cell population was identified by using the side and forward scatter Histogram and a Gate P1 was set. Only signals in this gate were further used for quantification. The uptake of particles into cells was measured by using the fluorescence signal normalized to the intrinsic signal of the cells. Furthermore, a side scatter analysis was done to check for increased granularity. Granularity is a measure of the inner structure of cells, whereby a high granularity, indicated by high side scatter values, indicates structural inclusions. Therefore, a side scatter analysis is often used to indicate particle uptake into cells [29, 30].

Statistical analysis

Statistical analysis was performed using SigmaPlot 14.0 (Systat Software GmbH, Erkrath, Germany). For cytotoxicity assays, one-way ANOVA following Dunnett's test was used, thereby comparing untreated medium controls with cells that were treated with respective nano- or microplastic particles. Statistical analysis as well as means and standard deviations were performed for at least three independent experiments. The significance levels were defined by performing one-way ANOVA Dunnett's test and calculating p-values ($^* = p < 0.05$, $^{**} = p < 0.01$, $^{***} = p \leq 0.001$).

Results

Characterization of submicro- and nanoplastic particles

To characterize the physicochemical properties of environmentally relevant particlesused as test materials in this study, a variety of analytical methods (fluorescence microscopy, SEM, DLS, assessment of octanol-water distribution coefficient, AF4 and SAXS) were applied (Fig. 1). The aim was to characterize and quantify the size range distribution between single-digit micrometer particles and down to the nanoscale.

Fluorescence microscopy was used to detect fluorescently labeled particles of different sizes and shapes (Fig. 1A), and was complemented by the use of SEM, which provided more detailed information regarding particle size and shape (Fig. 1B and C, respectively). PLA2000, described by the supplier to have a size of 2 µm, is represented by spherical particles characterized by a broad size range of between 200 nm and 10 µm in diameter. PLA250 consisted of smaller irregular shaped particles, characterized as being between 70 and 200 nm. An important observation, is that the PLA250 particles tended to agglomerate and form bigger particles. MF366 is characterized as representing the most monodisperse group of spherical particles used in this study, with a narrow particle size distribution at about 300 nm. PMMA25, anticipated to be characterized by individual particles

(See figure on next page.)

Fig. 1 Characterization of particles. **A** Fluorescence microscopy. **B** SEM. **C** Diameter analysis of SEM images. Dotted lines indicate diameters specified by the manufacturer. n.d. = not detectable. **D** DLS measurements of at least two samples and calculated values for hydrodynamic diameter and polydispersity index of 1:1000 diluted stock dispersions. **E** Zeta Potential of at least three samples of 1:1000 diluted stock dispersions. **F** Distribution of particles in hydrophilic (water) and lipophilic (octanol) phases after 0 h and 24 h incubation. Error bars indicate standard deviation of independent experiments ($n = 3$). **G** AF4 coupled to Multi Angle and Dynamic Light Scattering (MALS/DLS) **H** SAXS data of PMMA particles and a curve fit utilizing a log-normal size distribution of the diameters (left, black circles and red solid line, respectively). The intensity of the data around $q = 0.5\ nm^{-1}$ decays with about q^{-3} (indicated by arrow and a blue dotted line). Size distribution corresponding to the curve fit in the left-hand pane (right). Displayed is the partial differential function (PDF, red line) and cumulative distribution functions (CDF, black dashed line)

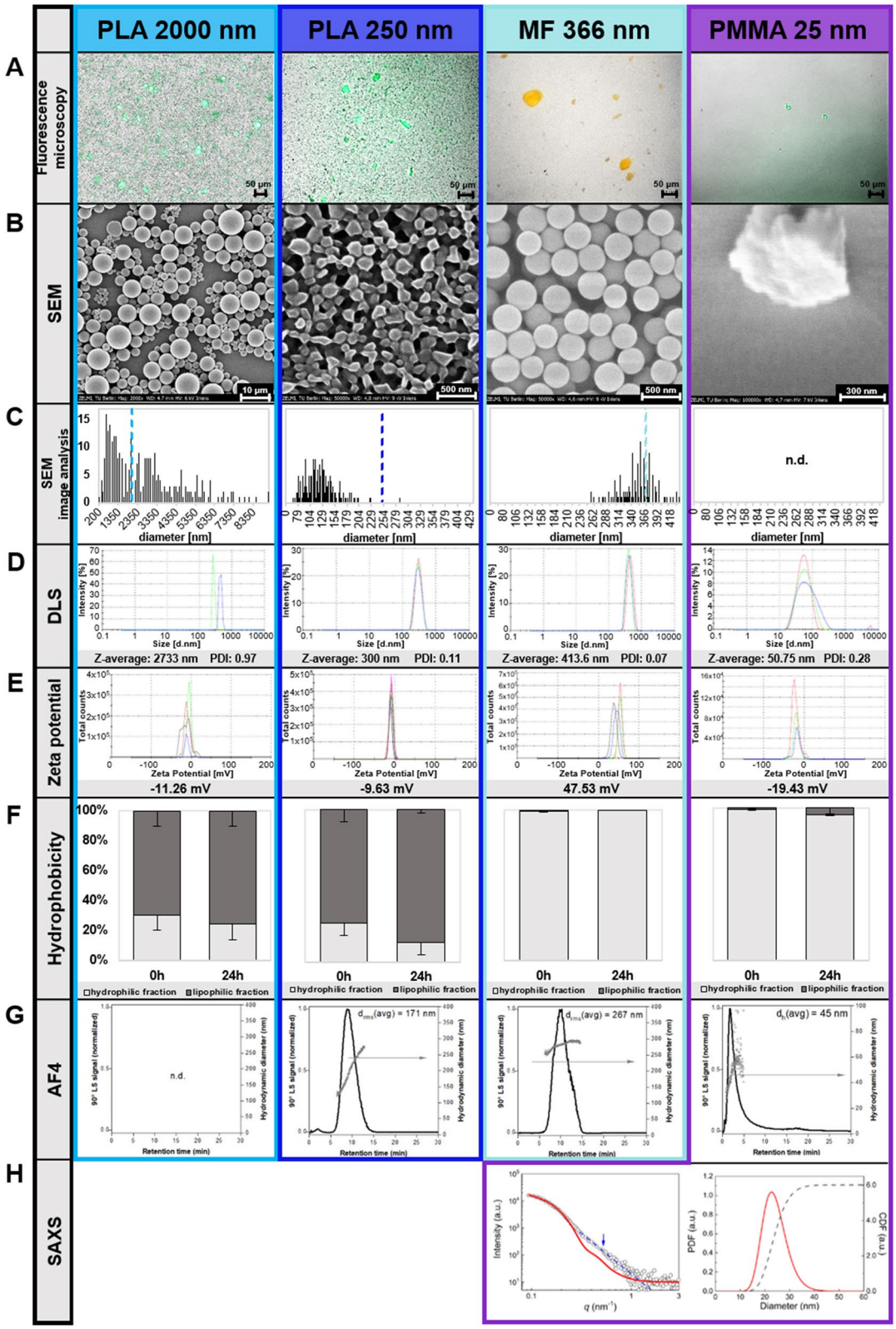

Fig. 1 (See legend on previous page.)

in the nanometer size range, resulted in particles visible by SEM that were limited to larger particle aggregates (approx. 600–800 nm diameter), with a negligible number of individual free particles being observed. The presence of single particles, however, was observed by DLS, AF4 and SAXS measurements, with a mean diameter of 38 nm for individual PMMA25 particles.

DLS measurements were used to check for the hydrodynamic diameter and the zeta potential of the particles (Fig. 1D and E, respectively). For PLA2000, DLS displayed a hydrodynamic diameter of 2733 nm, and a high polydispersity index (PDI) of 0.97. The PDI gives information about the distribution of particle sizes in the applied sample ranging from 0 to 1 (0 ≙ homogenous distribution, 1 ≙ polydispersed sample) [31]. Due to the high polydispersity observed for PLA2000, especially the DLS, which has limitations, caution may be warranted when attempting to interpret results. PLA250, on the other hand, resulted in an observed hydrodynamic diameter of 300 nm and a PDI of 0.11. MF366 measurements resulted in the lowest PDI of 0.07, and a mean hydrodynamic diameter of 413.6 nm. Moreover, the DLS was able to measure non-aggregated PMMA nanoparticles, which resulted in an observed hydrodynamic diameter of 50.75 nm and a PDI of 0.26. The zeta potential of both the PLA and PMMA particles was negative, between − 10 to − 20 mV, whereas MF366 showed a positive zeta potential of around 50 mV. The results of the DLS measurements in cell culture medium were comparable to those in ultrapure water (Table S3).

To determine the hydrophilic/hydrophobic character of the test particles, the dispersions were incubated in an octanol-water mixture and fractionation was measured in a plate reader after 0 h and 24 h (Fig. 1F). Both PLA particles showed nearly the same behavior, as the vast majority was detected in the lipophilic phase in a time-dependent manner. In contrast to that, MF366 and PMMA25 did not pass over to the lipophilic phase but stayed in the hydrophilic phase after both incubation time points of 0 h and 24 h, respectively.

Separation by AF4 was tested in carrier liquids containing small amounts of either the alkaline detergent mix FL-70, or the anionic surfactant SDS. Both are commonly used in AF4 analysis. Separation was possible for PLA250, MF366 and PMMA25 in carrier liquid containing FL70 (Fig. 1G). Online MALS provided average d_{rms} values across the peak of 171 nm for PLA250 and 267 nm for MF366. Assuming a solid sphere, this would correspond to geometric diameters of 221 nm and 345 nm, respectively, which is in good agreement with the nominal sizes. For PLA250, d_{rms} increased with retention time across the peak from 120 nm to 275 nm, confirming a proper elution of the particles in the AF4 channel (i.e., according to AF4 theory). For MF366, d_{rms} only slightly increased from 250 to 295, and was in agreement with the narrow size distribution of the particles. The relative broad peak width (despite the monomodal particle character) and the fact that the peak eluted at a similar retention time as the smaller PLA250 particles, suggests some degree of non-ideal elution behavior. Due to the small particle size, online DLS was applied for PMMA25 and average d_h of 45 nm determined which was in agreement with the (offline) DLS results. Particle size increased across the peak from 24 nm to 96 nm. In the carrier liquid containing SDS, strong particle-membrane interaction of PLA250nm was observed. Despite repeated injections of the sample, no material eluted (Fig. S1). This might be related to the observed hydrophobic character of the particles. Separation of MF366 was possible after several injections of the sample and resulted in a shouldered peak (Fig. S1). PMMA25 could be separated without the need for membrane pre-saturation and an average d_h of 40 nm was determined (Fig. S1). PLA2000 was not analyzed by AF4 as particles with sizes below and above the steric inversion point were present, which makes meaningful separation impossible [32]. Steric inversion is the process when normal-mode separation (smallest particles elute first) begins to convert to steric-mode separation (largest particles elute first). As a rule of thumb particles of between 1 and 1000 nm are separated in normal mode and particles > 1 to ~ 1000 µm are separated in steric mode.

SAXS, suitable for the characterization of particles below 100 nm in size, was employed to determine the size distribution of the PMMA nanoparticles (sample p_1). The SAXS curve of p_1 displays a characteristic Guinier region at $q < 0.2\,nm^{-1}$, which is typical for non-interacting particles, and therefore we can largely exclude aggregates (Fig. 1H). We conclude that the particle aggregates seen in the SEM figure most likely resulted from the preparation of the particles for analysis by SEM. The scattering curve is interpreted using the analytical form factor of a sphere with a log-normal number-weighted size distribution of the diameter (for details see experimental section). Equation (1) was employed for interpretation of the scattering data of p_1 resulting in a fit curve shown in Fig. 1H (red solid line). It can be seen that the model fit the data well in the low q-range but not at intermediate values around $q = 0.5\,nm^{-1}$ (indicated by an arrow). The scattering intensity in this intermediate region decays approximately with q^{-3} (blue dotted line) which is much lower than q^{-4} as must be expected for particles with a smooth surface. A possible interpretation for the q^{-3}-scaling can be a rough interface between the PMMA particles and their surroundings, e.g. approximately describable as surface fractal. However, there is not enough information to

confirm this. The distribution of the particles' number density as probability density function (PDF) and cumulative density function (CDF) is shown in Fig. 1H (red solid and black dashed curves in the right-hand panel). The median diameter is $D_{median} = 23.6 \pm 0.2$ nm and the mean is $D_{mean} = 24.1 \pm 0.3$ nm. The standard deviation of the width of the diameter distribution is about 5 nm (20% of D_{mean}).

Effects on intestinal and liver cells

Cellular effects were determined using MTT and xCELLigence® assays (Fig. 2). In the MTT assay (Fig. 2A), particles were applied at concentrations between 2.5×10^7 and 2.5×10^{10} µm^2 particle surface/mL for 24. The cytotoxicity measurements are used to screen for cell viability, and to identify toxic and non-toxic concentrations over in a wide concentration range.

When applied to differentiated Caco-2 cells, most test particles were observed to have no impact on cell viability. Only the highest concentration of MF366 (2.5×10^{10} µm^2 particle surface/mL) resulted in a significantly reduced ($p < 0.01$) cell viability. On HepG2 cells, the MF366 and PLA250 test particles showed significant toxic effects ($p < 0.001$), while on HepaRG cells, only MF366 had a significant impact on cell viability at the two highest concentrations. The nanoplastic PMMA25 particles and the larger microplastic PLA2000 particles are observed to have no adverse effects on any cell line in the applied concentration range. In contrast, the xCELLigence® method is more sensitive and allows real-time measurements over a defined time period (Fig. 2B). Selected concentrations used for the MTT test were chosen for this assay. As a positive control, ZnO particles were used, and were observed to show a significant decrease ($p < 0.001$) of the relative cell index on all cell lines during the experimental test period. There were almost no other effects detected on Caco-2 cells. Only PLA250 showed a significant decrease ($p < 0.001$) of cell viability at the highest used concentrations (1×10^{10} and 2.5×10^{10} µm^2 particle surface/mL). The impact on liver cells was much higher. For the submicron test particles MF366 and PLA250 a dose-dependent and statistically significant toxic response over the time on HepG2 cells was observed in the xCELLigence® assay. The other test particles PLA2000 and PMMA25 did not evoke negative changes in the relative cell index. On HepaRG cells, a reduction of the relative cell index was elicited by the MF366 and PLA250 test particles, while PLA2000 and PMMA25 had no influence on the relative cell indices.

Uptake and transport of submicro- and nanoplastics using fluorescence microscopy

The cellular particle uptake and transport was investigated using the Caco-2 Transwell® model (Fig. 3). In addition, the uptake of particles into liver cell models (HepG2, HepaRG) was determined (Fig. 4). High, but non-toxic concentrations, which exceed human consumption, were applied.

To check for permeability of the cells, TEER was measured and P_{APP} values calculated (Figs. S2 and S3). No decreases in cell permeability were detected. For the intestinal barrier, representative fluorescence and confocal microscopic images showed variances in uptake quantity and cellular particle distribution (Fig. 3A and B, respectively). A distinct difference of intracellular localization between (almost same-sized) submicron test particles MF366 and PLA25 was observed. While MF366 tended to form agglomerates in the cellular interior (yellow/red signal), PLA250 appeared to envelop the cellular membrane and to adhere to the cell surface (green/red signal). Nevertheless, confocal microscopy showed for both particle types that the membrane was unimpaired. Only the large agglomerates of MF366 were able to destroy the cellular membrane, most likely influenced by their size. For PLA2000, only a limited number of particles were detected at the surface of the cells or were absorbed into the cell. It was obvious that only the smaller particles of the dispersion were able to penetrate the cell membrane. In contrast, almost no PMMA25 single particles were detected on or in Caco-2 cells. This can be explained by the size resolution limit of the microscope, which has a particle size limit of detection at 200 nm. Still, no particle agglomerations were observed in the samples, as they are too big to cross cellular membranes. For instance, the pore size of the membrane (3 µm) is assumed to represent the upper size limit for particle transport.

The quantitative analysis for cellular interaction and transport of particles with and through differentiated Caco-2 cells was in good accordance with the microscopic images (Fig. 3C and D, respectively). For PLA2000, approximately 20% of the fluorescence signal was observed in the membrane fraction, indicating

(See figure on next page.)

Fig. 2 Cellular effects of particles on Caco-2 (left), HepG2 (middle) and HepaRG cells (right). **A** MTT Assay of increasing concentrations of particles after 24 h incubation time. 0.01% Triton X-100 was used as positive control. **B** Cellular impedance measurements using xCELLigence® system. Cell indices normalized to cell culture medium are shown over a time of 72 h. 50 µg/mL ZnO nanoparticles served as positive control. Data are presented as means ± standard deviation. The significance was calculated by performing one-way ANOVA Dunnett's test (* = $p < 0.05$, ** = $p < 0.01$, *** = $p \leq 0.001$, $n = 3$)

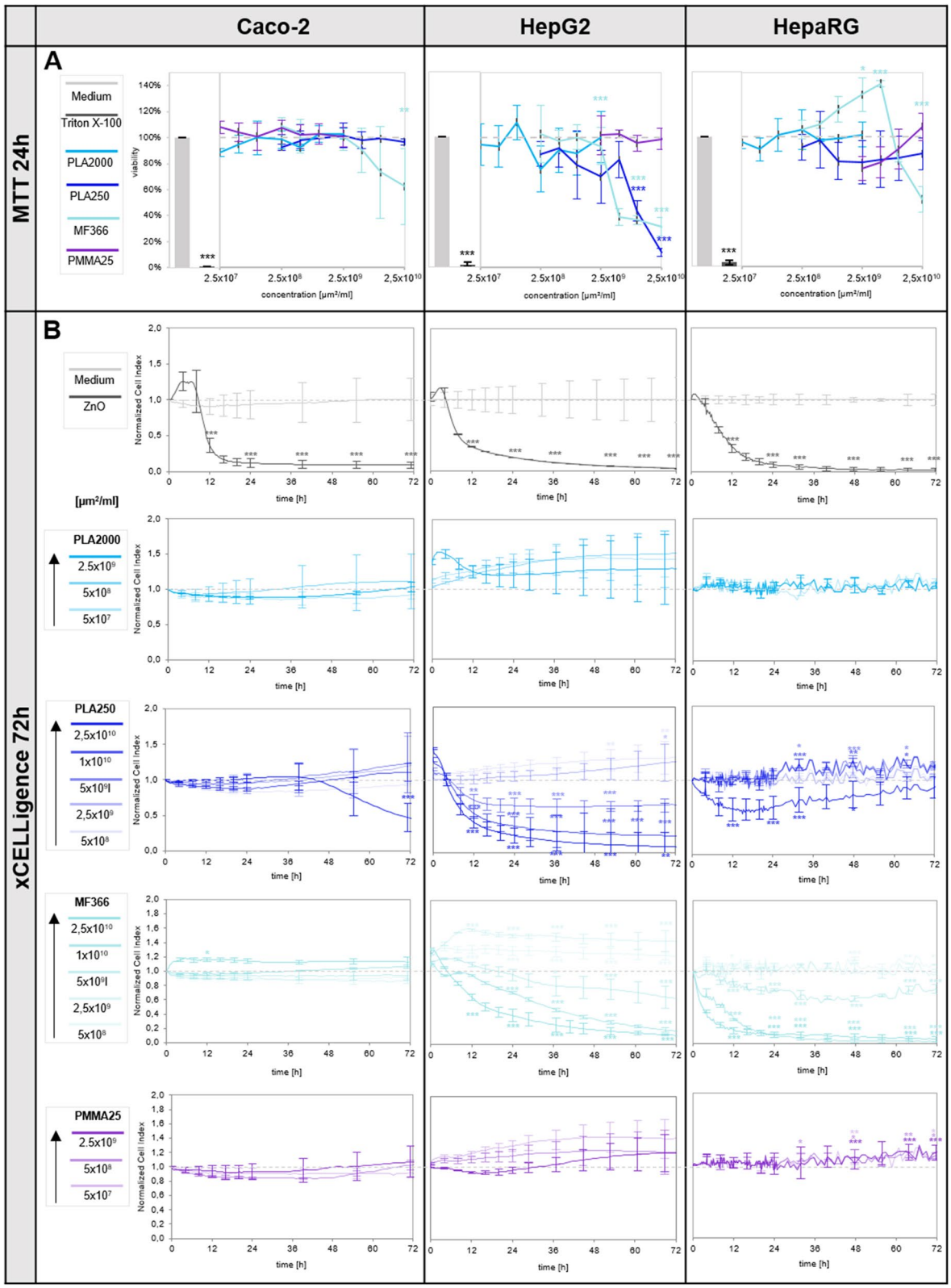

Fig. 2 (See legend on previous page.)

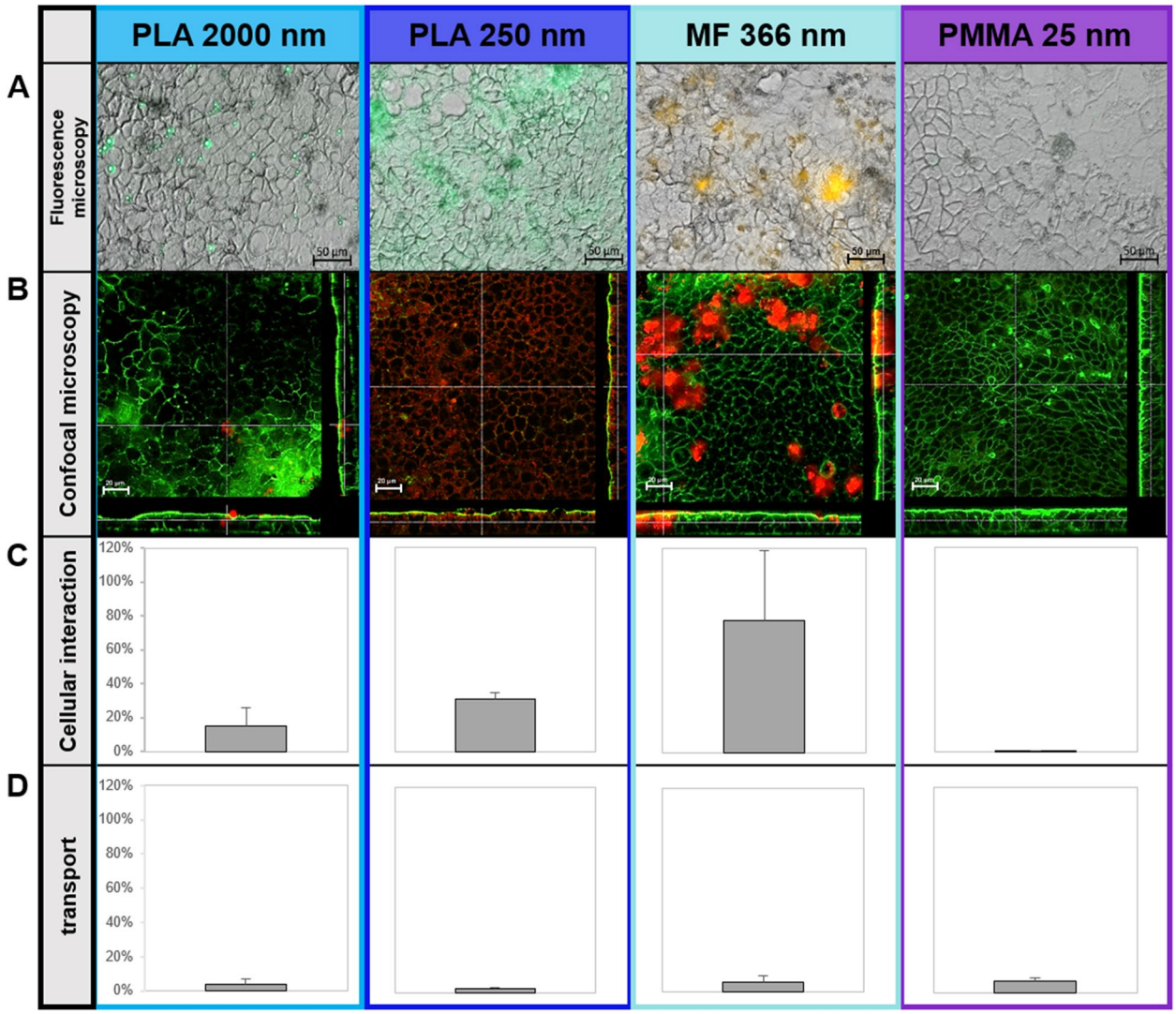

Fig. 3 Analysis of uptake and transport of particles through the intestinal epithelial Caco-2 cell monolayer after 24 h incubation in a Transwell® system. **A** Representative fluorescence microscopic images. Gray spots indicate the Caco-2 cells and colored spots indicate particles. **B** Representative confocal microscopic images. Green spots indicated the Caco-2 Monolayer and red spots the particles. **C** Fraction of particles interacting with the Caco-2 cell monolayer (uptake or laying on top of the cells) determined with a plate reader. **D** Percentage of particles transported through the Caco-2 cell monolayer determined with a plate reader. Data are shown as mean values ± standard deviation of three independent experiments

the potential uptake of smaller particles. The remaining 80%, however, was observed in the apical compartment, while less than 3% are reported as crossing the epithelium membrane. Interestingly, the cellular interaction of the similar sized submicron test particles MF366 and PLA250 was different for the different polymer types. Specifically, 30% of the incubated PLA250 test particles were observed as being homogenously distributed across the cellular fraction. In contrast, MF366 was quantified to have a cellular interaction of 75%, thereby exhibiting a high standard deviation, most likely influenced by the agglomerates causing a high fluorescence signal. Both submicron test particles (PLA250 and MF366) were observed to be similarly transported through the intestinal barrier, at between 2 and 4%. It was not possible, however, to detect PMMA25 via fluorescence quantification in the cellular fraction, although it is worth noting that about 6% was detected in the basolateral compartment.

In the liver cells, only microscopic evaluation was performed (Fig. 4). The two liver cell lines (HepG2 and HepaRG) showed similar results, which are also comparable to the cellular interaction patterns of the particles

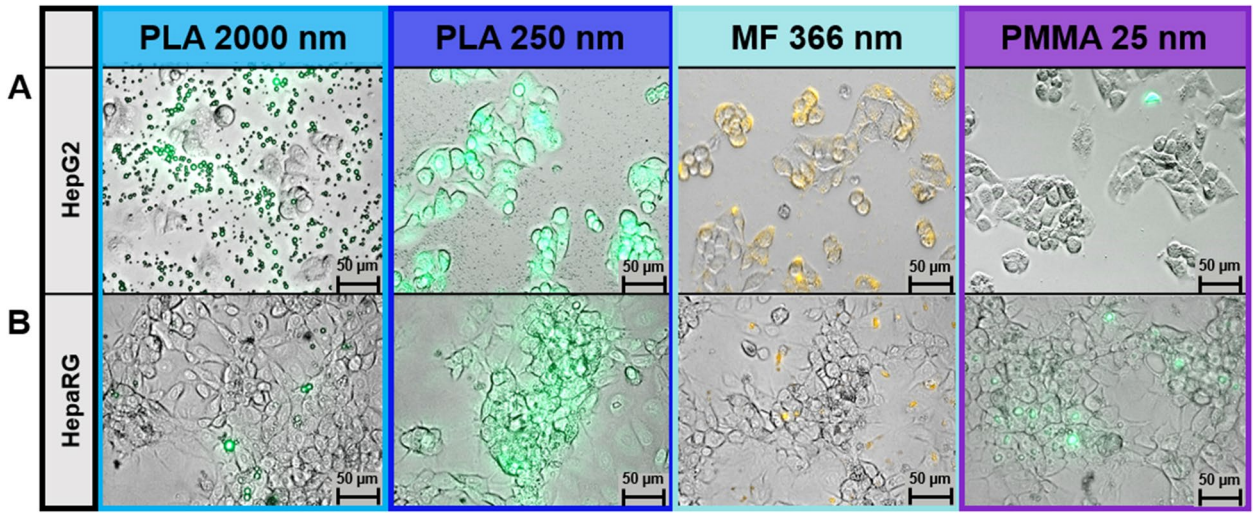

Fig. 4 Representative fluorescence microscopic images of particles after 24 h incubation with **A**: HepG2 and **B**: HepaRG cells. Gray structures indicate the cells and colored structures the particles

with the Caco-2 cells. For PLA2000, many particles surrounded the HepG2 cells, but only a relatively small fraction was observed to be taken up by HepG2 and HepaRG cells. Again, only the smaller part of the dispersion was detected in/on the cells. Surprisingly, the nanoplastic test particles showed the same variance in uptake and particle distribution as for the Caco-2 cells. PLA250 surrounded the whole cell membrane of both liver cell lines, whereas MF366 was observed to be localized only in parts of the cells, where formation of agglomerates in the cellular interior was also observed. For PMMA25, it was possible to detect rarely occurring particle accumulations, especially in HepaRG cells, from which, compared to the other test particles, the least uptake of particles was observed.

Quantification of uptake of submicro- and nanoplastics via flow cytometry

Another possible method to measure particle uptake is through the use of flow cytometry. Fluorescent particles can be detected inside the cells by emitting significantly higher fluorescence than cells without particles. We established the method using previously characterized fluorescent PS particles [23] and determined their cellular uptake into HepG2 cells as a simple model for liver cells (Fig. S4). The particles had sizes of 1, 4 and 10 µm, respectively. The fluorescence threshold was defined using the upper limit of background fluorescence without the application of particles. To monitor the increase of particle uptake, a kinetic study was performed and samples were taken after 2, 4, 6 and 24 h of incubation. Complementary to the flow cytometric quantification is the use of optical microscopy, whereby microscopic images were also taken and evaluated.

Fluorescence microscopy showed that only 1 and 4 µm particles were taken up into the cells, while 10 µm particles were too large to be taken up (Fig. S4). The observations are consistent with results from flow cytometry measurements of the fluorescence detected in the cells. For PS 10 µm, no uptake of particles was detected within 24 h. In contrast to that, the uptake of PS 4 µm was quantified at 11.2% and for PS 1 µm at 66.4%. It was further possible, to count the number of incorporated PS microplastic particles which appeared in distinct single population peaks. Results from the kinetic study, not only demonstrated that the general fluorescence signal of incorporated particles increased with decreasing particle size, but also that the number of particles taken up by one cell increased in a time-dependent manner. For PS 4 µm, 1.5% of the cells had taken up > 3 particles and 9.5% of the cells had taken up between 1 and 2 particles after 24 h incubation. PS 1 µm was absorbed in higher values. It is clear that the HepG2 cells incorporated an increasing number of particles with longer incubation times. After 24 h, 16.5% of the cells had taken up 5 and more particles, 15% between 3 and 4 particles and around 35% between 1 and 3 particles.

After having established the model with PS particles, the 4 particle types investigated in this study were tested. All of them showed different behavior (Fig. 5). Instead of different identifiable populations that enable to quantify the uptake of the number of particles per cell, the overall fluorescence distribution changed only to

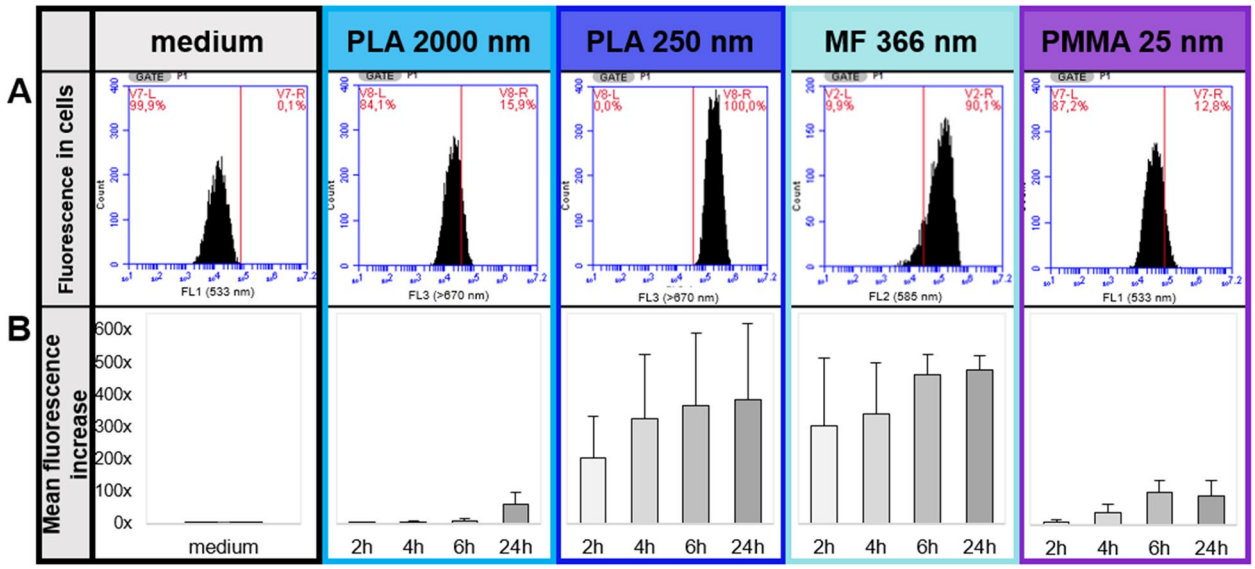

Fig. 5 Quantification of uptake of particles in HepG2 cells after 24 h (**A**) and 2, 4, 6, 24 h (**B**) incubation. **A** Representative Histograms depicting the count of fluorescence signals dependent on the fluorescence intensity. The vertical red line shows the division between intrinsic fluorescence of the cells (see medium) and increasing fluorescence signals after particle uptake. The percentage of the uptake is depicted in the upper right corner. **B** Mean fluorescence increase after incubation of HepG2 with particles after 2, 4, 6, and 24 h incubation, respectively. Quantification was determined related to medium. Data are shown as means ± SD, $n = 3$

higher values in one broad peak (Fig. 5A). In the kinetic study, the mean fluorescence over all cells increased during a period of 24 h (Fig. 5B). For PLA2000, the uptake increased from 2x to 70x in comparison to the medium. The highest uptake values were detected for the submicron particles. Already after 2 h, a 236x or 349x higher signal was detected for PLA250 and MF366, respectively. These signals increased after 24 h up to 441x or 551x, respectively. Nevertheless, the standard deviations were quite high. PMMA25 also showed an increasing uptake from 13x to 102x within 24 h of incubation.

Another method to determine and characterize particle uptake is a side-scatter analysis (Fig. 6). Only in the instance of MF366 particles was there an observed strong increase of the side scatter. Cells incubated with the other test particles (PLA250 and PLA2000 (data not shown), PMMA25 (data not shown)) showed only a minor or no increase of signals. This increase in granularity is supposed to be related to the particle uptake, because the highest side scatter signals (red) were detected in the highest fluorescence intensity cell fraction (cells that have taken up the highest amount of particles).

Discussion

The topic of MNPs has been increasingly studied in the last decade, resulting in a need to better understand the potential relationships between the physicochemical properties of the particles and the possible health impacts that might accompany their ingestion. Due to various challenges, such as a lack of appropriate reference materials, analytical methods and challenges associated with characterizing exposure and effects for particles < 10 µm, evaluating human health risks is currently limited. An important element towards better understanding the implications that exposure to MNPs may represent to human health is a need to better understand the systemic uptake and cellular effects of environmentally relevant particles. For instance, cellular uptake, increased bioavailability and the disturbance of cellular processes are more likely to increase as particle size decreases, largely because nanoplastic particles, in particular, are understood to have a higher probability to permeate the gastrointestinal barrier more effectively than larger microplastic particles [25, 33].

This study aims to contribute to the understanding of essential differences between microplastic and nanoplastic particles, with an emphasis on evaluating fate and effects in cellular systems relevant to an oral ingestion pathway. Therefore, micro- (> 1 µm) submicro- (1000–100 nm) and nanoplastic (< 100 nm) particles with relevance to exposure via contamination of food and beverages were used. In a first step, particles were characterized and toxic effects measured. The second step comprised quantification of cellular interaction of particles with Caco-2 cells (mimicking the intestinal barrier), HepaRG and HepG2 cells, respectively (mimicking liver

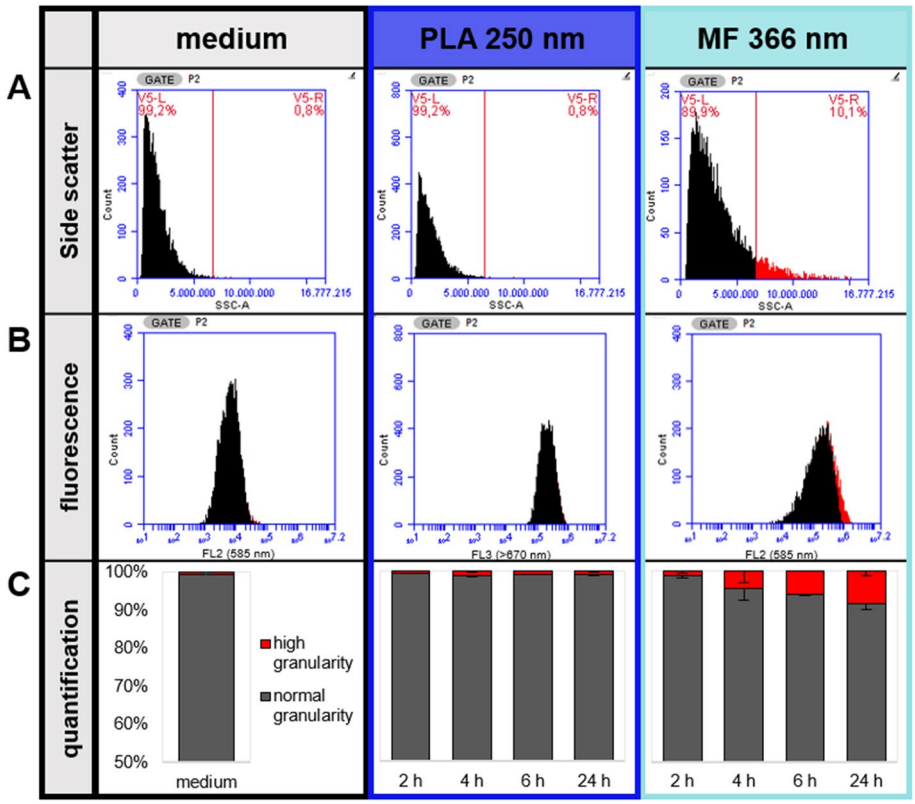

Fig. 6 Side scatter analysis of PLA250 and MF366 after 2, 4, 6 and 24 h incubation with HepG2 cells. **A** Representative Histograms of signals detected by the side scatter after 24 h incubation. The vertical red line shows the threshold between normal cell granularity and increased granularity due to particle uptake (red). **B** Representative Histograms of measured fluorescence signal correlating to (**A**). Red labeled counts show cells with high side scatter. **C** Quantification of the increase of the side scatter after 2, 4, 6 and 24 h incubation. Cells with high granularity are depicted in red and cells with normal granularity in gray. Data are shown as means ± SD, $n = 2$

cells) as well as transport through the intestinal barrier. In the last step, a flow cytometry-based method was established and successfully applied to analyze the uptake of submicron- and nanoplastic particles into HepG2 cells.

The characterization of PLA2000 resulted in broadly distributed particles between 10 µm and the lower nanometer size range. For PLA250, the size distribution was much narrower, but particles aggregated due to SEM preparation steps, which resulted in irregular shapes. The slightly negative zeta potential indicated a reasonable colloidal stability in the dispersion. The MF particles, on the other hand, exhibited the narrowest size distributions, the most spherical shape and the zeta potential was strongly positive. The behavior of the nanometer-sized PMMA25 particles was more complicated. Using SEM and confocal microscopy, only particle aggregates were visible, but the application of alternative analytical methods were sufficient to identify distinct nanoparticles with sizes between 24 and 50 nm. It is important to underline that measurements of zeta potential are used to assess the relative stability of a particle dispersion in a solvent. It does not necessarily correlate to particle functionalization or surface charge. When diluting the particles in cell culture medium, the particle surface will be rapidly covered with organic matter [34]. Consequently, it is important that a variety of properties and analytical techniques be measured and used for determining the stability of the test particle dispersion. For instance, since fluorescent plastic particles of different materials were used, their distribution in hydrophilic or lipophilic phases needs to be elucidated, as this facilitates to evaluate fate and behavior in different types of solvents and culture media. PLA250 accumulated more in the lipophilic phase and MF366 was observed to remain in the hydrophilic fraction. This can have influence on particle-cell interactions [35]. The test particles included in this study are thus observed to include a diverse range of properties. PLA2000 test particles represented larger microplastic particles with a broad particle size distribution, and are consistent with a polydisperse suite of properties. The different properties of the PLA200 particles are anticipated to behave differently with respect to cellular uptake, bioavailability and

effects increasing with decreasing particle size. PLA250 and MF366, on the other hand, represent test particles of different polymeric composition, both characterized by particle sizes in the submicrometer size range, but with contrasting hydrophobicity behavior, whereas PMMA25 was used to represent nanoparticles of < 100 nm, and which are a food-relevant material.

With regard to fluorescence measurements, the potential for analytical artifacts needs to be taken into consideration. For instance, fluorescence interferences with other wavelengths can occur, such as in experiments with fluorometric readouts, therefore efforts to limit and account for interferences must be implemented. Additionally, cellular autofluorescence might lead to overestimation of the fluorescence intensity [36], whereas, the leaching of fluorophores from the particles can also result in an overestimate of uptake. Concerns related to the leaching of fluorophores is well documented, such as can be seen in the study of Catarino et al. [36], who demonstrated that the fluorophores of fluorescently labeled nanometer PS detached from the particle, which then entered and agglomerated in the tissue of zebrafish larvae. To avoid misinterpretations in relation to interferences and autofluorescence, we have selected test particles with fluorescence spectra unlikely to be consistent with other interfering wavelengths, which has been further evaluated through the use of negative controls in all experiments. Similarly, efforts have been implemented to account for the potential of fluorophore leaching, whereby test particles were subject to ultracentrifugation experiments prior to use, aimed at minimizing leaching in both aqueous and organic test media. Verification demonstrated that in both cases, there was no leaching of fluorophores.

Measurements of acute and long-term cellular toxicity of submicro- and nanoplastic particles revealed a statistically significant viability decrease ($p < 0.001$) for PLA250 and MF366 for the highest test concentrations after 24 h, which were verified in the xCELLigence® assay. These results are confirmed by other *in vitro* toxicity studies with PET, PS, PP and PE microplastics, which detected no cytotoxicity [37–39] or cytotoxicity only in likely unphysiological situations [23, 24, 40, 41]. Furthermore, Fröhlich et al. [42] reported that the smaller the nanoparticle, the more cytotoxic effects are reported for phagocytic cells, which is consistent with our findings [42]. Given that the test concentrations of plastic particles used in this study, and which resulted in adverse effects, are likely significantly greater than those estimated in relation to human exposure, it is unlikely that environmental concentrations would represent a significant risk. Cox et al. [3], for instance, estimated that Americans ingest an amount of microplastics ranging from 39,000–52,000 particles per year [3], concentrations that are far below the applied *in vitro* concentrations in our study ($> 2 \times 10^6$ particles/mL), implying that the conclusion that decreasing viability only arises due to an indirect effect, such as when cells are not able to take up nutrients due to particle overload, and not because of effects arising from the plastic material itself. It should be noted, however, that we have performed the screening experiments reported in this study to identify the highest non-toxic concentrations that can be applied for use when evaluating physiological uptake.

Cellular interaction, uptake and transport of the test particles using a model of the intestinal barrier was evaluated. A transport ranging from 2 to 6%, varying depending on plastic particle size and material composition, was observed. The integrity of the Caco-2 monolayer was not impaired due to particle incubation as shown by TEER and P_{app} values. Regarding the interaction of MNPs with enterocytes, we observed particle- size-, −material and -surface-dependent effects. PLA2000, representing polydisperse microplastics, interacted with the monolayer, with the smaller size particles taken up by cells and particles > 4 µm remaining on the surface of the cells. This is consistent with other studies, examining the uptake of microplastic particles [23, 24]. For the two test particles in the submicrometer range (PLA250 and MF366), higher cellular interactions, characterized by different distribution and behavior were observed. The smallest nanoplastic particles (PMMA25), did not measurably interact with the monolayer, which is possibly because the particles are able to cross the barrier more efficiently due to their small size and transported to the basolateral side, a suggestion that is consistent with their observation as having the highest quantified transport of 6% [43]. Possible mechanisms of particle uptake include paracellular transport, persorption or endocytosis [35]. Other studies investigating uptake and transport using the Caco-2-based barrier model have reported similar results. Stock et al. [23], for instance, exposed 1, 4 and 10 µm sized PS particles for 24 h to the barrier model and detected a cellular interaction up to 3%, but unquantifiable transport of particles. The largest uptake rates were surprisingly reported for PS 4 µm [23]. As shown by our work, cellular interaction and transport increases with decreasing particle size. This observation is in agreement with Kulkarni & Feng et al., who detected a time-dependent increase of uptake of PS particles smaller than 500 nm [44]. Interestingly, other colleagues quantified a high transport (14%) of sulfonated 50 nm PS particles after 24 h exposure and internalization into lysosomes of Caco-2 cells [39]. Other studies quantified highest transport for 50 nm and 100 nm PS nanoplastics, which are especially negatively charged [45]. Stock

et al. [25] measured uptake and transport of differently sized and coated nanometer PS. A size- and surface-dependent particle uptake was quantified. This implies differences of cellular uptake in relation to differences in surface charge and particle size, which is in concordance with other findings for particles in the submicrometer range (PLA250 and MF366) as they exhibit different surface properties [45, 46]. By using PET nanoplastics with 100 nm in size, Magri et al. detected a small time-dependency in relation to uptake and transport through Caco-2 cells over nine days of incubation, but reported no toxic effects such as LDH release, decreasing cell viability, reactive oxygen species production or apoptosis/necrosis [37]. Others used 50 nm PS particles and exposed undifferentiated Caco-2 cells for eight weeks, simulating a sub-chronic exposure to nanoplastics. They reported accumulation of particles in cells, small changes in genotoxic markers, but no DNA damage or oxidative stress [47].

Given the important function of the intestinal barrier for absorbing nutrients from food, while at the same time preventing the systemic distribution of potentially harmful substances [48], the enterocytes build up a strong semipermeable barrier connected with tight junctions. When discussing results arising from Caco-2-based models, it is important to consider that they are known to often lead to underestimated results in comparison to the *in vivo* situation, because the monolayer exhibits a denser barrier than human epithelial cells, due to strong tight junctions [49]. Nevertheless, we observed a noteworthy transport of all particles through the Caco-2 intestinal cells, suggesting the potential for the particles to reach the liver. The question thus arises regarding the fate and effects of MNPs in relation to liver cells. Applying a flow cytometry-based method and fluorescence microscopy, a time-dependent uptake especially for PLA250 and MF366 was measured, but, in contrast to PS, no distinct number of incorporated particles per cell could be determined. Interestingly, uptake of aggregated PMMA25 was also detected, which suggests a higher susceptibility of liver cells for the uptake of substances in comparison to intestinal cells. What needs to be additionally considered, however, is how an increase in fluorescence measured by flow cytometry correlates with both, the single particle fluorescence intensity and the number of particles taken up by one cell might be interpreted. For instance, in the absence of considering how to best interpret fluorescence measurements, there is the potential for an over−/underestimated uptake to be observed. To obtain reliable and comparable results, the method needs to be validated with other analytical techniques for each applied particle species. For example, Gottstein et al. combined confocal microscopy with flow cytometry for the quantification of 50 nm and 1 µm PS uptake, aimed at providing a more accurate and precise quantification [50]. In our study, the results are in a good concordance with the flow cytometry data.

Many *in vivo* feeding studies have been conducted to examine uptake and systemic bioavailability of microplastics in organs such as intestine, liver, gut, kidney and spleen. By applying 1, 4 and 10 µm PS particles to mice for 28 days, another study investigated no bioaccumulation or other adverse effects have been detected. Only some particles were found in the intestine, but not in the liver [23]. A study by Jani et al. documented systemic bioavailability for particles with diameters in the submicrometer range [51, 52]. In our study, we reported the highest transport through intestinal cells and uptake in liver cells for MF366 and PMMA25, which supports the hypothesis of a higher systemic bioavailability for smaller particles. Overall, it can be summarized that past *in vitro* and *in vivo* studies consistently observe time-dependent uptake that increases with decreasing particle size, which can be further influenced by differences in particle surface properties.

The side scatter analysis, reported in this study, suggests significant changes in the granularity of HepG2 after uptake of MF366, for which noteworthy differences in the octanol-water distribution were also observed. This suggests altered mechanisms of uptake and interactions with cell membranes after exposure to MF366, caused by e.g. differences in hydrophobicity and material [35, 43, 46, 53–55]. Liu et al. [43] examined uptake mechanisms of 50 nm and 500 nm PS exposed to leukemia cells and model membranes. The particles were taken up via passive membrane interaction (hydrophobic interactions) and active endocytosis (size-dependent types of uptake) and accumulated in in the lysosomes of cells. A study from Li et al. [46] pointed out that hydrophobic particles are able permeate into the membrane bilayer but did not affect the tightness of the membrane. On the other hand, more hydrophilic particles only adsorb on the surface and do not enter the cells. Moreover, simulation of relevant mammalian cell lipid membranes showed mechanical stretching following exposure to PE (1 and 10 µm), PS (800 nm) and PMMA (1 and 8 µm) test plastic particles leading to destabilization of the membrane and structural changes especially after accumulation of particles [53]. Concerning our study, it is important that future studies aim at trying to elucidate the underlying uptake and transport mechanisms of test particles, especially for PLA250 and MF366. To date, there are no other studies that have investigated the possible adverse health effects of these environmentally relevant materials, thus research that expands beyond the use of PS particles will only help strengthen our overall understanding of the

human health implications that exposure to MNPs represents. It can be hypothesized that PLA250 and MF366 interact differently with Caco-2, HepaRG and HepG2 cells due to differences in hydrophobicity and surface charge. For PLA250 it can be suggested that the particles interact with the cell membrane and MF366 are taken up actively by endocytosis.

Conclusion

We applied food-relevant plastic particles of different sizes to an *in vitro* model of the intestinal barrier and to liver cells. There are strong differences observed with respect to fate and effects. Cellular uptake increases with decreasing particle size, which can also vary depending on the composition of the polymer. This is most likely influenced by lipophilic interactions with the cellular membrane. A higher fraction of the hydrophilic MF particles are observed to permeate the cell membrane and form detectable aggregates in cellular cavities, whereas the lipophilic PLA250 particles, of almost the same size, were observed to be distributed across the cell membrane and likely intercalate into the lipid layer. In this case, particles in the submicrometer range behaved in accordance to their physicochemical surface properties than as expectable for a particle in the micrometer range. PMMA25 nanoplastic particles also distributed all over the cell surface, especially in liver cells. Regarding toxicological effects, the submicro- and nanoplastic particles showed a higher impact on the cells, when compared with the apparently more unreactive microplastic particles. This can be due to size- but also material-dependent mechanisms, which could disturb the smooth running of cellular processes, while bigger microparticles were incorporated without having a noteworthy cellular impact.

Our findings underline the importance of the topic of nanoplastics. Even though nanoplastics are known to be unreactive due to their chemical structure, they can disturb cellular functions without reacting themselves but by interaction with the cellular membrane [53, 56] or possibly by adsorbing substances e.g. acting as Trojan horse [57]. These effects are especially important after agglomeration of nanoplastics. Additionally, the question arises whether nanoplastics are able to reach deeper organs besides the intestine due to an altered cellular fate [51, 52]. This strongly indicates the necessity of investigations on submicron and nanoscaled fractions of particulate plastic particles, which due to increased surface-to-volume-ratio and a tendency for increasing cellular uptake with decreasing particle size, suggests the importance of considering the impact of size, shape, surface, overall chemistry and hydrophobicity.

Abbreviations

AF4: Asymmetric Flow Field Flow Fractionation; CDF: Cumulative density function; DLS: Dynamic Light Scattering; DMEM: Dulbecco's Modified Eagle Medium; DMSO: Dimethylsulfoxide; EDTA: Ethylenediaminetetraacetic acid; FCS: Fetal calf serum; FITC: Fluorescein isothiocyanate-dextran; MALS: Multi Angle Light Scatttering; MF: Melamine formaldehyde; MNPs: Micro- and nanoplastic particles; MTT: 3-(4,5-dimethylthioazole-2-zyl)-2,5-diphenyltetrazolium bromide; P/S: Penicillin/Streptomycin; PBS: Phosphate-buffered saline; PDF: Probability density function; PDI: Polydispersity index; PLA: Polylactic acid; PMMA: Polymethyl-methacrylate; PS: Polystyrene; SAXS: Small-angle X-ray Scattering; SDS: Sodium dodecyl sulfate; SEM: Scanning Electron Microscopy; TEER: Transepithelial electrical resistance.

Supplementary Information

The online version contains supplementary material available at https://doi.org/10.1186/s43591-022-00036-0.

Additional file 1.

Acknowledgements

The authors thank Marén Schlief and Sandra Graff for technical assistance. We further thank M. Ebisch for SAXS experiments.

Authors' contributions

MP 1,2,3,4: Cellular Studies, Uptake, Effects, Fluorescence Microscopy, flow cytometry. CF 1,2: SEM. LG 1,2: AF4. TH 1,2: Cellular Studies, Uptake, Effects, Fluorescence Microscopy, flow cytometry. KL 1,2: AF4. LB 2,3,4. AFT 1,2: SAXS. AB 3,4,5. HS 2,3,4. 1) Performed experiments, 2) Data Evaluation, 3) Writing the Manuscript, 4) Project Planning, 5) Supervision and Funding. The author(s) read and approved the final manuscript.

Funding

Open Access funding enabled and organized by Projekt DEAL. This project was funded by the German Federal Institute for Risk Assessment, Germany (projects 1323–102, 1322–782 and 1329–003-1222214) in cooperation with the Technical University of Denmark (DTU) and the Federal Institute for Materials Research and Testing (BAM).

Availability of data and materials

All data generated or analyzed during this study are included in this published article and its supplementary information files.

Declarations

Competing interests

The authors declare that they have no competing interests.

Author details

[1]Department of Food Safety, German Federal Institute for Risk Assessment, Max-Dohrn-Str. 8-10, 10589 Berlin, Germany. [2]Technical University of Berlin, Center for Electron Microscopy (ZELMI), Straße des 17. Juni 135, 10623 Berlin, Germany. [3]Technical University of Denmark, Research Group for Analytical Food Chemistry, Kemitorvet 201, 2800 Kgs. Lyngby, Denmark. [4]Division Synthesis and Scattering of Nanostructured Materials, Federal Institute for Materials Research and Testing (BAM), Unter den Eichen 87, 12205 Berlin, Germany.

Received: 19 January 2022 Accepted: 22 May 2022
Published online: 17 June 2022

References

1. Vethaak AD, Legler J. Microplastics and human health. Science. 2021;371(6530):672–4.
2. Schymanski D, Goldbeck C, Humpf HU, Furst P. Analysis of microplastics in water by micro-Raman spectroscopy: Release of plastic particles from different packaging into mineral water. Water Res. 2018;129:154–62.

3. Cox KD, Covernton GA, Davies HL, Dower JF, Juanes F, Dudas SE. Human consumption of microplastics. Environ Sci Technol. 2019;53(12):7068–74.
4. Yee MSL, Hii LW, Looi CK, Lim WM, Wong SF, Kok YY, et al. Impact of microplastics and nanoplastics on human health. Nanomaterials-Basel. 2021;11(2):496.
5. Schymanski D, Humpf HU, Furst P. Determination of particle abrasion through milling with five different salt grinders - a preliminary study by micro-Raman spectroscopy with efforts towards improved quality control of the analytical methods. Food Addit Contam A. 2020;37(8):1238–52.
6. Jin M, Wang X, Ren T, Wang J, Shan J. Microplastics contamination in food and beverages: Direct exposure to humans. J Food Sci. 2021;86(7):2816–37.
7. EFSA. Presence of microplastics and nanoplastics in food, with particular focus on seafood. EFSA J. 2016;14(6):e04501.
8. Paul MB, Stock V, Cara-Carmona J, Lisicki E, Shopova S, Fessard V, et al. Micro- and nanoplastics - current state of knowledge with the focus on oral uptake and toxicity. Nanoscale Adv. 2020;2(10):4350–67.
9. Senathirajah K, Attwood S, Bhagwat G, Carbery M, Wilson S, Palanisami T. Estimation of the mass of microplastics ingested - A pivotal first step towards human health risk assessment. J Hazard Mater. 2021;404(Pt B):124004.
10. Mohamed Nor NH, Kooi M, Diepens NJ, Koelmans AA. Lifetime Accumulation of Microplastic in Children and Adults. Environ Sci Technol. 2021;55(8):5084–96.
11. Hernandez LM, Xu EG, Larsson HCE, Tahara R, Maisuria VB, Tufenkji N. Plastic teabags release billions of microparticles and nanoparticles into tea. Environ Sci Technol. 2019;53(21):12300–10.
12. Li D, Yang L, Kavanagh R, Xiao L, Shi Y, Kehoe DK, et al. Sampling, identification and characterization of microplastics release from polypropylene baby feeding bottle during daily use. J Vis Exp. 2021;173.
13. Zangmeister CD, Radney JG, Benkstein KD, Kalanyan B. Common Single-Use Consumer Plastic Products Release Trillions of Sub-100 nm Nanoparticles per Liter into Water during Normal Use. Environ Sci Technol. 2022;56(9):5448–55.
14. Schymanski D, Ossmann BE, Benismail N, Boukerma K, Dallmann G, von der Esch E, et al. Analysis of microplastics in drinking water and other clean water samples with micro-Raman and micro-infrared spectroscopy: minimum requirements and best practice guidelines. Anal Bioanal Chem. 2021;413(24):5969–94.
15. Oßmann BE. Microplastics in drinking water? Present state of knowledge and open questions. Curr Opin Food Sci. 2021;41:44–51.
16. Krug HF, Wick P. Nanotoxicology: an interdisciplinary challenge. Angew Chem Int Ed Engl. 2011;50(6):1260–78.
17. Gouin T, Ellis-Hutchings R, Thornton Hampton LM, Lemieux CL, Wright SL. Screening and prioritization of nano- and microplastic particle toxicity studies for evaluating human health risks - development and application of a toxicity study assessment tool. Microplast nanoplast. 2022;2(1):2.
18. van Raamsdonk LWD, van der Zande M, Koelmans AA, Hoogenboom R, Peters RJB, Groot MJ, et al. Current insights into monitoring, bioaccumulation, and potential health effects of microplastics present in the food chain. Foods. 2020;9(1):72.
19. Kooi M, Koelmans AA. Simplifying microplastic via continuous probability distributions for size, shape, and density. Environ Sci Tech Let. 2019;6(9):551–7.
20. Volkheimer G. Passage of particles through the wall of the gastrointestinal tract. Environ Health Perspect. 1974;9:215–25.
21. Hartmann NB, Huffer T, Thompson RC, Hassellov M, Verschoor A, Daugaard AE, et al. Are we speaking the same language? recommendations for a definition and categorization framework for plastic debris. Environ Sci Technol. 2019;53(3):1039–47.
22. Koelmans AA, Besseling E, Shim WJ. Nanoplastics in the aquatic environment. Critical review. Mar Anthropogenic Litter. 2015:325–40.
23. Stock V, Böhmert L, Lisicki E, Block R, Cara-Carmona J, Pack LK, et al. Uptake and effects of orally ingested polystyrene microplastic particles in vitro and in vivo. Arch Toxicol. 2019;93(7):1817–33.
24. Stock V, Laurisch C, Franke J, Donmez MH, Voss L, Bohmert L, et al. Uptake and cellular effects of PE, PP, PET and PVC microplastic particles. Toxicol Vitro. 2021;70:105021.
25. Stock V, Bohmert L, Coban G, Tyra G, Vollbrecht ML, Voss L, et al. Microplastics and nanoplastics: Size, surface and dispersant - What causes the effect? Toxicol Vitro. 2022;80:105314.
26. Kammer FVD, Baborowski M, Friese K. Field-flow fractionation coupled to multi-angle laser light scattering detectors: Applicability and analytical benefits for the analysis of environmental colloids. Anal Chim Acta. 2005;552(1–2):166–74.
27. Bressler I, Kohlbrecher J, Thunemann AF. SASfit: a tool for small-angle scattering data analysis using a library of analytical expressions. J Appl Crystallogr. 2015;48(Pt 5):1587–98.
28. Luckert C, Schulz C, Lehmann N, Thomas M, Hofmann U, Hammad S, et al. Comparative analysis of 3D culture methods on human HepG2 cells. Arch Toxicol. 2017;91(1):393–406.
29. Sieg H, Ellermann AL, Maria Kunz B, Jalili P, Burel A, Hogeveen K, et al. Aluminum in liver cells - the element species matters. Nanotoxicology. 2019;13(7):909–22.
30. Zucker RM, Massaro EJ, Sanders KM, Degn LL, Boyes WK. Detection of TiO2 nanoparticles in cells by flow cytometry. Cytometry A. 2010;77(7):677–85.
31. Danaei M, Dehghankhold M, Ataei S, Hasanzadeh Davarani F, Javanmard R, Dokhani A, et al. Impact of particle size and polydispersity index on the clinical applications of lipidic nanocarrier systems. Pharmaceutics. 2018;10(2):57.
32. Kammer F, Legros S, Hofmann T, Larsen EH, Loeschner K. Separation and characterization of nanoparticles in complex food and environmental samples by field-flow fractionation. TrAC Trends Anal Chem. 2011;30(3):425–36.
33. Saptarshi SR, Duschl A, Lopata AL. Interaction of nanoparticles with proteins: relation to bio-reactivity of the nanoparticle. J Nanobiotechnology. 2013;11:26.
34. Bohmert L, Voss L, Stock V, Braeuning A, Lampen A, Sieg H. Isolation methods for particle protein corona complexes from protein-rich matrices. Nanoscale Adv. 2020;2(2):563–82.
35. Behzadi S, Serpooshan V, Tao W, Hamaly MA, Alkawareek MY, Dreaden EC, et al. Cellular uptake of nanoparticles: journey inside the cell. Chem Soc Rev. 2017;46(14):4218–44.
36. Catarino AI, Frutos A, Henry TB. Use of fluorescent-labelled nanoplastics (NPs) to demonstrate NP absorption is inconclusive without adequate controls. Sci Total Environ. 2019;670:915–20.
37. Magrì D, Sánchez-Moreno P, Caputo G, Gatto F, Veronesi M, Bardi G, et al. Laser Ablation as a Versatile Tool To Mimic Polyethylene Terephthalate Nanoplastic Pollutants: Characterization and Toxicology Assessment. ACS Nano. 2018.
38. Lehner R, Wohlleben W, Septiadi D, Landsiedel R, Petri-Fink A, Rothen-Rutishauser B. A novel 3D intestine barrier model to study the immune response upon exposure to microplastics. Arch Toxicol. 2020;94(7):2463–79.
39. Abdelkhaliq A, van der Zande M, Punt A, Helsdingen R, Boeren S, Vervoort JJM, et al. Impact of nanoparticle surface functionalization on the protein corona and cellular adhesion, uptake and transport. J Nanobiotechnology. 2018;16(1):70.
40. Stock V, Bohmert L, Donmez MH, Lampen A, Sieg H. An inverse cell culture model for floating plastic particles. Anal Biochem. 2020;591:113545.
41. Hesler M, Aengenheister L, Ellinger B, Drexel R, Straskraba S, Jost C, et al. Multi-endpoint toxicological assessment of polystyrene nano- and microparticles in different biological models in vitro. Toxicol in Vitro. 2019;61:104610.
42. Frohlich E, Meindl C, Roblegg E, Griesbacher A, Pieber TR. Cytotoxity of nanoparticles is influenced by size, proliferation and embryonic origin of the cells used for testing. Nanotoxicology. 2012;6(4):424–39.
43. Liu L, Xu K, Zhang B, Ye Y, Zhang Q, Jiang W. Cellular internalization and release of polystyrene microplastics and nanoplastics. Sci Total Environ. 2021;779:146523.
44. Kulkarni SA, Feng SS. Effects of particle size and surface modification on cellular uptake and biodistribution of polymeric nanoparticles for drug delivery. Pharm Res. 2013;30(10):2512–22.
45. Walczak AP, Kramer E, Hendriksen PJ, Tromp P, Helsper JP, van der Zande M, et al. Translocation of differently sized and charged polystyrene nanoparticles in in vitro intestinal cell models of increasing complexity. Nanotoxicology. 2015;9(4):453–61.
46. Li Y, Chen X, Gu N. Computational investigation of interaction between nanoparticles and membranes: hydrophobic/hydrophilic effect. J Phys Chem B. 2008;112(51):16647–53.

47. Domenech J, de Britto M, Velazquez A, Pastor S, Hernandez A, Marcos R, et al. Long-term effects of polystyrene nanoplastics in human intestinal Caco-2 cells. Biomolecules. 2021;11(10):1442.
48. Vancamelbeke M, Vermeire S. The intestinal barrier: a fundamental role in health and disease. Expert Rev Gastroenterol Hepatol. 2017;11(9):821–34.
49. Hilgendorf C, Spahn-Langguth H, Regardh CG, Lipka E, Amidon GL, Langguth P. Caco-2 versus Caco-2/HT29-MTX co-cultured cell lines: permeabilities via diffusion, inside- and outside-directed carrier-mediated transport. J Pharm Sci. 2000;89(1):63–75.
50. Gottstein C, Wu GH, Wong BJ, Zasadzinski JA. Precise quantification of nanoparticle internalization. ACS Nano. 2013;7(6):4933–45.
51. Jani P, Halbert GW, Langridge J, Florence AT. The uptake and translocation of latex nanospheres and microspheres after oral administration to rats. J Pharm Pharmacol. 1989;41(12):809–12.
52. Jani P, Halbert GW, Langridge J, Florence AT. Nanoparticle uptake by the rat gastrointestinal mucosa: quantitation and particle size dependency. J Pharm Pharmacol. 1990;42(12):821–6.
53. Fleury JB, Baulin VA. Microplastics destabilize lipid membranes by mechanical stretching. Proc Natl Acad Sci U S A. 2021;118(31):e2104610118.
54. Nel AE, Madler L, Velegol D, Xia T, Hoek EM, Somasundaran P, et al. Understanding biophysicochemical interactions at the nano-bio interface. Nat Mater. 2009;8(7):543–57.
55. Bouwmeester H, Hollman PC, Peters RJ. Potential Health Impact of Environmentally Released Micro- and Nanoplastics in the Human Food Production Chain: Experiences from Nanotoxicology. Environ Sci Technol. 2015;49(15):8932–47.
56. Holloczki O, Gehrke S. Can nanoplastics alter cell membranes? Chemphyschem. 2020;21(1):9–12.
57. Hildebrandt L, Nack FL, Zimmermann T, Pröfrock D. Microplastics as a Trojan horse for trace metals. J Hazard Mater Lett. 2021;2:100035.

Publisher's Note